# Optimal control of a heat pump-based energy system for space heating and hot water provision in buildings: results from a field test

Brida V. Mbuwir[1,2,*], Davy Geysen[1,2], George Kosmadakis[3], Marika Pilou[3], George Meramveliotakis[3], Hermen Toersche[4]

[1]Flemish Institute for Technological Research (VITO), Mol, Belgium
[2]EnergyVille, Genk, Belgium
[3]Thermal Hydraulics and Multiphase Flow Laboratory, National Centre for Scientific Research "Demokritos", Agia Paraskevi, Greece
[4]Thermovault, Leuven, Belgium
[*]Corresponding author: brida.mbuwir@vito.be

## Abstract

This paper presents and discusses results from a field test that uses model predictive control (MPC) to optimise the operation of a multi-source heat pump-based energy system for space heating and hot water provision in a building. The objective of the optimisation is to minimise the electricity consumption of the heat pump using flexibility from the heat sources, the space heating and domestic hot water tanks while ensuring end-user comfort and system constraints. The field test was performed in the context of the RES4BUILD project that developed a system consisting of: photovoltaic-thermal (PVT) collectors, an innovative vapour-compression multi-source heat pump (with a solar buffer connected to the PVT collectors, a borehole thermal energy storage and air as heat sources) and water buffer tanks for serving the space heating and hot water needs of the building. The optimal operation of the system is obtained by monitoring and controlling the interactions between the different system components using MPC, taking into account the weather and heating demand forecasts. Results have shown that MPC has a potential and added value for the optimal operation of multi-source heat pumps in real-life while considering system constraints and user behaviour to ensure thermal comfort. However, significant effort and expert knowledge are needed to develop the sufficiently accurate system models required by this control approach. The outcomes and conclusions of this work are therefore a basis for further development of such control approaches to improve their replicability and feasibility on a large scale, considering the diverse nature of energy system components in buildings.

**Keywords:** buildings, domestic hot water, field test, heat pump, model predictive control, optimisation, PVT collectors, space heating

## Nomenclature

### Abbreviations

| | |
|---|---|
| AI | Artificial Intelligence |
| BEMS | Building Energy Management System |
| BTES | Borehole Thermal Energy Storage |
| COP | Coefficient Of Performance |
| DHW | Domestic Hot Water |
| EU | European Union |
| HP | Heat Pump |
| MPC | Model Predictive Control |
| PLC | Programmable Logic Controller |
| PVT | Photovoltaic-Thermal |
| SH | Space Heating |

### Symbols

| | |
|---|---|
| $k$ | Control time step index, [-] |
| $P_{HP,HEAT}$ | Daily electricity consumption of the heat pump for space heating, [kWh/day] |
| Q | Domestic hot water or space heating demand, [kW] |
| $\dot{Q}$ | Thermal power of heat pump, [kW] |
| $\tilde{Q}$ | Heat of heat pump for charging a tank, [kW] |
| T | Temperature, [°C] |
| $z_{cd}$ | Binary control that selects which tank the HP charges, [0/1] |
| $z_{ev,air}$ | Binary control that selects evaporator source air, [0/1] |
| $z_{ev,btes}$ | Binary control that selects evaporator source BTES, [0/1] |
| $z_{ev,solar}$ | Binary control that selects evaporator source solar buffer, [0/1] |
| $z_{pvt}$ | Binary control that selects what the PVT charges, [0/1] |

### Subscripts

| | |
|---|---|
| b | Solar buffer tank |
| btes | BTES tank |
| cd | Condenser |
| dhw | DHW tank |
| ev | Evaporator |
| in | Inlet |
| oper | Operational |
| out | Outlet |
| set | Setpoint |
| sh | Space heating tank |
| ∞ | Ambient |

## 1. Introduction and related work

Energy for heating and cooling accounts for more than 50% of the total final energy consumption in the European Union (EU), with only 23% of this energy coming from renewable energy sources [1]. Thus, decarbonising the heating and cooling sector is crucial for meeting the EU target of at least 55% net greenhouse gas emissions reductions and 45% renewable energy target by 2030 [2]. To this end significant work has been done on the development of more efficient heat pumps and photovoltaic-thermal (PVT) systems for buildings [3] [4], [5]. In fact, the recent energy crisis accelerated the efforts towards energy efficiency, energy savings and efficient integration of renewable energy sources into the heating and cooling sector.

Energy efficiency and savings can be achieved by reducing energy consumption for heating and cooling. One way of achieving this reduction is by minimizing the building energy requirements using more efficient thermal insulation for the building envelope [6] with the help of building information modelling [7]. This improves the thermal energy storage capacity of the building while reducing energy losses to the environment. Energy consumption for heating and cooling can equally be reduced via optimal energy management strategies, which control the heating and cooling systems [8] [9] [10]. Therefore, building energy management systems (BEMS) implementing optimal control strategies are needed to achieve the required energy efficiency and energy savings via monitoring and control of the heating and cooling system while ensuring thermal comfort for the users. At the building level, flexibility in energy consumption can be extracted not only from heat pump installations with thermal storage for space heating and hot water provision, but also from devices with electric energy storage capacity such as electric batteries.

In recent years, there has been a surge in the use of model predictive control (MPC) for optimal control of heat pumps for heating and cooling [11]–[23]. A significant portion of these works have focused on the implementation of MPC in a simulation environment to control the operation of heat pumps, with the objective of maximising self-consumption of local renewable energy generation, reducing electricity cost or achieving energy savings. Most of the heat pumps use either air or ground as their low temperature heat source. Even though a significant amount of work has been done in the literature for optimising the operation of single-source heat pumps using MPC, research on optimal control of multi-source heat pumps using MPC remains limited both at theoretical and practical level.

Research on multi-source heat pumps (with ambient air, geothermal energy, or solar/PVT collectors as heat sources) has recently gained popularity in the effort to decarbonise heating/cooling in buildings. Several theoretical and experimental studies have been carried out to evaluate the performance of these heat pumps via simulations [24]–[27]. These simulations have shown that multi-source heat pumps achieve high efficiencies while remaining economically viable. The claims via simulation have been supported via monitoring and detailed analysis of data collected from real-life operation of these systems in buildings. The work of Busato et al. [29] concluded that the integration of different sources not only increases the thermal performance of the system as a whole, but also optimises the use of each source and more energy savings could be obtained by controlling the indoor temperature setpoints. The conclusions from this study have also been supported by the work of Lazzarin et al. [28] who highlighted the benefits of multi-source heat pumps in a real-life operation through the analysis of five years data from a multi-source heat pump system operating in a school building. This work emphasized on the importance of system monitoring to ensure the expected energy savings are achieved, particularly when the system integrates multiple technologies in the long term.

Besides developments on theoretical and experimental aspects to evaluate the performance and viability of multi-source heat pumps, significant progress has also been made towards a controlled operation of heat pump-based energy systems to improve their energy performance [29], [30].

Weeratunge et al. [29] investigated a solar-assisted ground source heat pump for serving the heating needs of a building. The heat hump had two heat sources: the ground and a hot water tank that stores heat from the solar collectors. In the investigated system, an electric heater was also connected to the hot water tank to charge the tank during off-peak periods using electricity from the main grid. The authors used MPC for optimal operation and selection of the heat pump sources with the objective of minimising the electricity cost of the system. In the context of the SunHorizon project [31], Roure et al. [30] developed an MPC-based controller to optimise the operation of a solar-assisted heat pump system consisting of a hybrid PVT system, a gas-driven heat pump and a hot water storage tank. The aim of the optimization was to minimise $CO_2$ emissions and maximize the use of energy generated by the renewable energy source. Even though the aforementioned MPC developments for controlling the operation of heat pump-based energy systems are simulation-based, they have shown the potential of MPC for an optimised multi-source heat pump operation. While the use of MPC for multi-source heat pump control in real-life scenarios is still minimal, several field tests have been done using rule-based control [28], [32]–[34].

In the FlexHeat 2017 KAAECT project [32], a multi-source heat pump-based energy system was installed in a school building for serving its heating/cooling energy needs. The low temperature heat source consisted of ground heat exchangers, a ventilation heat recovery system and solar thermal collectors. In the field test, a rule-based controller was deployed to select the most suitable input source for the heat pump at every control interval with objective of achieving a near zero energy building target. The set of rules were based on the temperature of the water from the solar collectors and the ground. If the temperature of water from the solar system was higher than the ground temperature, the water from the solar system was used in the heat pump evaporator. However, if the solar system was off or the water temperature was not sufficiently high, the heat pump used the ground as the source. Similar rules were used in the experimental work carried out by Kaygusuz et al. [34] to switch between air and water input sources based on a fixed temperature called the switch-over temperature. The authors showed the effectiveness of rule-based control via an improved heat pump performance.

As part of the IDEAS project [35], a multi-source heat pump using PVT collectors, air and the ground as heat sources was used to meet the heating/cooling needs of a building [33]. An artificial intelligence (AI)-based technique for controlling the operation of the heat pump and different energy assets was developed to maximise the use of renewable energy production for heating, and cooling of the building via optimal demand side management. One main advantage of AI-based control techniques is that they are data-driven and rely mainly on the data collected from the system. Thus, eliminating the need for developing sufficiently accurate system models as in the case of MPC or crafting out a set rules as is the case of rule-based control. Through monitoring and analysis of the data collected from the system operation, the authors showed the effectiveness of multi-source heat pumps for integration of renewable energy sources for building and cooling.

In the context of the EXCESS project [36], a multi-source heat pump with heat sources a borehole thermal energy system (BTES) and a tank connected to PVT collectors will be used to meet the heating/cooling needs of the pilot buildings. The project aims at using MPC to optimally decide the low temperature heat pump heat source for meeting the heating/cooling needs of the users with objective of reducing cost or energy imported from the grid depending on the needs of the pilot site [37]. The project is currently in the development phase and results on the MPC implementation or pilot operation are yet to be published.

The work presented in this paper is based on a field test carried out in the context of the RES4BUILD project [38]. The project focused on developing innovative technologies for decarbonising heating/cooling in buildings and achieving energy savings. Several actions ranging from more efficient PVT collectors [1] and multi-source heat pumps [3], [39] to BEMS were developed within the project.

This paper focuses on the control software in the BEMS for optimising the performance of the system towards energy savings. The software consists of an optimization algorithm that considers all the different system components: multi-source vapour-compression heat pump, PVT collectors and thermal storage tanks (for serving the space heating/cooling and hot water needs of the building). The optimal operation of the system is obtained by monitoring and controlling the interactions between the different components, considering the system and user constraints as well as the weather and heating demand forecasts. All these while keeping the global objective of minimising the electricity consumption of the heat pump in perspective.

This work differs from the previous works as MPC is used not in a simulation environment but in a field test to demonstrate its potential in the real-life operation of multi-source heat pump-based energy systems in buildings. Flexibility is provided from the heat sources of the heat pump (air, solar buffer heated by PVT collectors and a virtual BTES system) and from the space heating and domestic hot water (DHW) tanks to collectively optimise for least energy consumption of the heat pump. Lessons learned during the field test provide insights for future application of MPC for optimal control of multi-source heat pumps in buildings, incorporating different user behaviours, leveraging flexibility from other building components such as the building envelop and other optimization objectives such as self-consumption of local renewable energy generation.

The rest of the paper is structured as follows: Section 2 introduces the pilot system, Section 3 discusses the optimization problem formulation and control strategy and Section 4 presents and discusses the results from the field test. Finally, the conclusions and lessons learned are discussed in Section 5.

## 2. Pilot system

The energy system is based on a multi-source heat pump for heating and cooling a small well insulated office building at NCSRD campus in Athens, Greece. The surface area of this single-floor building is 103 $m^2$. This system was been developed and commissioned at the beginning of 2022 and then the long-term field testing was initiated. A detailed description is provided next along with the local (rule-based) control that was initially implemented to adjust the system operation.

### 2.1 System description

The system is characterised by its flexibility to adjust its heat sources and sinks, aiming to increase its performance. This adjustment is implemented by varying the position of several 3-way valves both at the water and refrigerant sides. Moreover, 4 PVT collectors are included that are installed on the building rooftop and produce both heat and electricity. This solar heat charges either the DHW tank or the solar buffer, while electricity is fed into the grid. By directing the solar flow to the solar buffer, the average collector temperature is kept relatively low (below 35 °C) which favours the thermal efficiency of the PVT collectors. At the same time, the heat pump can use warm water from this buffer tank as its heat source (max. temperature of 25 °C) to further increase its coefficient of performance (COP). Another heat source is the so called virtual BTES with this ground heat exchanger emulated with the use of a horizontal tank kept at a temperature of ≈18 °C, which is a typical ground temperature in Athens at a depth of 80 m. An air-source heat pump maintains the BTES tank temperature at the desired value.

The heat delivery to the building is achieved by circulating hot water from the space heating buffer tank to the 4 fan coils installed in the 4 main rooms of the building. A separate thermostat is installed in each room and controls the operation of the room's fan coil, based on temperature setpoints that have been fixed once receiving input from the building users. During the day (from 08:00 to 21:00), the room temperature is allowed to vary in the range of 20.5 - 21 °C, while during the night (from 21:00 to 08:00) a lower setpoint is used with the room temperature maintained within the range of 18 - 19 °C.

As mentioned before, the building hosts offices of NCSRD without any DHW consumption. Therefore, the hot water demand had to be emulated, which was accomplished by removing heat from the DHW tank with the same predefined profile followed every day. This tapping profile is based on the medium ("M") profile defined in the EN16147:2017 standard and has been adjusted to consider the month of the year and the location [39] . Therefore, during winter when the tap water temperature is low, the daily DHW demand is about 16-18% higher than the average of 5.845 kWh/day according to this standard. To follow the (adjusted) tapping cycles of this standard, a controllable electronic valve at the tap water inlet is allowed to open for a specific number of minutes (in total 33 minutes per day) spread across the day [40]. During those periods, the tap water flow rate is constant while a recirculation pump is engaged with a PID control to keep the tap outlet temperature as close as possible to the set value of 45 °C.

The system process diagram with the piping connections and all 3-way valves that adjust the operation is shown in Figure 1 at both heating and cooling mode. It should be stressed that only the results from the winter season are presented.

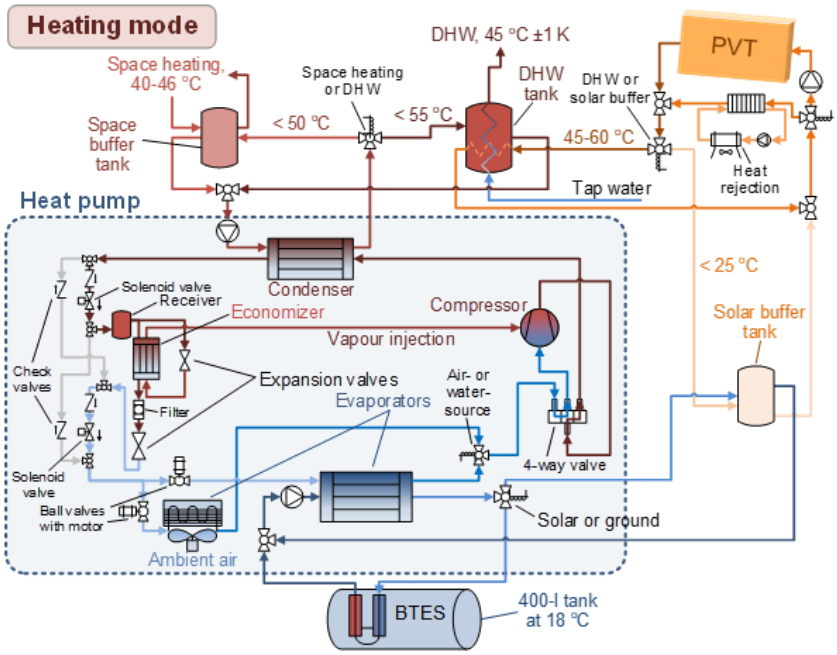

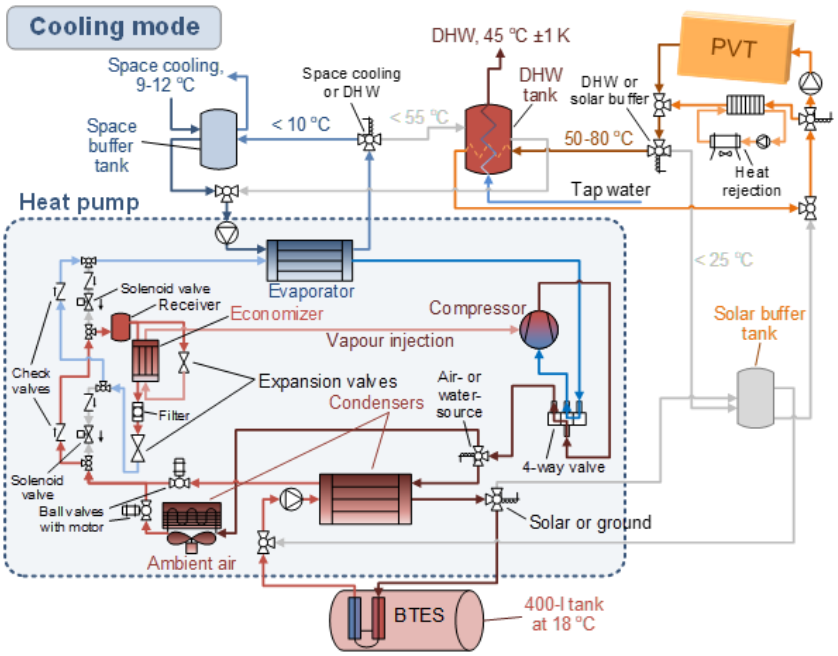


*Figure 1 System diagram at heating and cooling mode including piping and 3-way valves.*

The system flexibility originates from the selection of various heat sources and sinks. In heating mode, the heat sources are the following: (1) heat from the virtual BTES, (2) heat from the solar buffer, or (3) heat from the ambient air. The heat sinks at the condenser side of the heat pump are either the DHW tank or the space heating tank.

Two views of the installed energy system are shown in Figure 2, illustrating the containerized control room in which the heat pump and the DHW tank are located. All other components are placed outdoors. The 4 PVT collectors are mounted on the rooftop. The pumping box contains several water circulators, 3-way valves, sensors (temperature, flow rate) and a plate heat exchanger for removing heat from the solar circuit in case of overheating. A more detailed description of the system components and their main parameters can be found in [40]–[42].

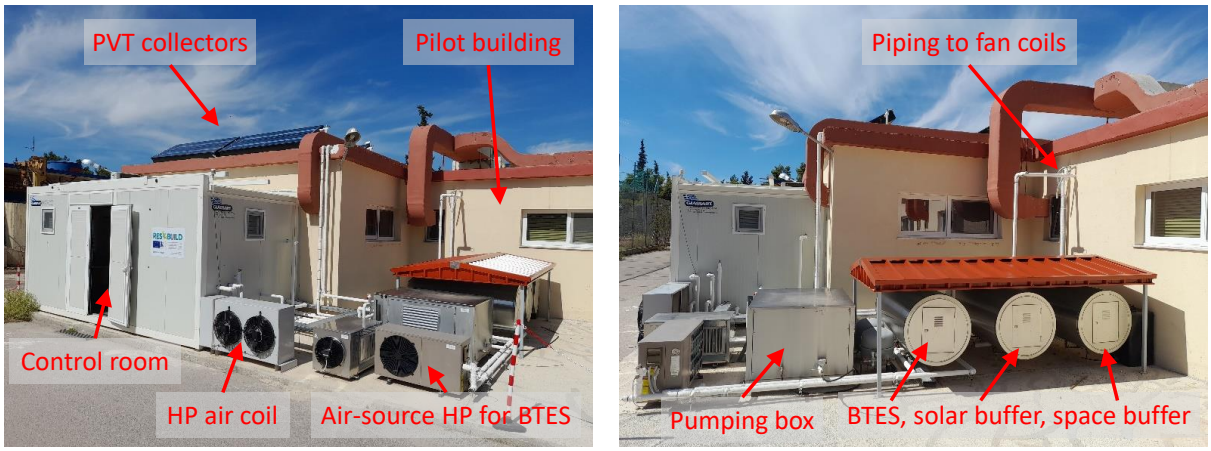


*Figure 2 Pilot system installation at NCSRD in Athens, indicating the main system components.*

The multi-source heat pump and the DHW tank are placed in the containerised control room, along with several sensors for measuring power, flow rate, pressure and temperature. The PLC unit of the heat pump executes the commands for several components while a separate (independent) controller is installed that puts into operation the fan coils circuit and the collector circuit.

## 2.2 Local control

A rule-based control has been developed to allow the system to run with all its functionalities during the first stages of testing. This control is also called local control because it is implemented within the PLC unit of the heat pump that monitors most parts of this system. The adjustment of the 3-way valve positions is achieved based on some rules that have been derived during the system simulation activities [41] with the setpoints of the heating load corresponding to the tank temperatures (shown in Figure 1). These rules are the following:

i. The solar flow of the collectors is directed to the solar buffer if this tank temperature is below 20 °C or is fully charged (at 25 °C). Otherwise, the 3-way valve at the collector circuit is directed towards the DHW tank.
ii. If both DHW and space heating tank request heat from the heat pump (i.e. tank temperature below its setpoint), priority is given to the DHW charging and once the setpoint is reached, the condenser 3-way valve is switched towards the space buffer.
iii. The heat source to the heat pump is the BTES tank if its temperature is higher than the solar buffer. Otherwise, the solar buffer provides heat to the cold side of the heat pump (air-source was not an option in that control version).

The system performance under the local control will be compared with the one obtained with the BEMS control that optimizes the system operation as described next.

# 3 Methodology – optimization problem and control strategy

As explained in the previous section, the pilot system has a vapour compression heat pump that supplies both the space heating (SH) and DHW tanks, which in turn serve these end-user needs, as shown in Figure 3. There are three heat sources to the evaporator of the heat pump: air, BTES (ground source) or solar buffer. Additionally, the PVT collectors can charge either the solar buffer or the DHW tank directly. The goal of the optimization problem is to make optimal control decisions on how much heat is taken from the different heat sources, i.e., what heat pump heat source should be used, which of the tanks (space heating or DHW) should be served and which tank (solar buffer or DHW) should be charged by the PVT collectors. The control decisions in the optimization can thus be summarised as follows:

- PVT collectors: serve the solar tank or DHW tank.
- Heat pump
    - ON/OFF
        - If ON
            - Which source should be used as heat input (outdoor air, BTES or solar buffer)
            - Which sink should the heat pump serve (space heating or hot water tank)
    - Temperature setpoint of the condenser

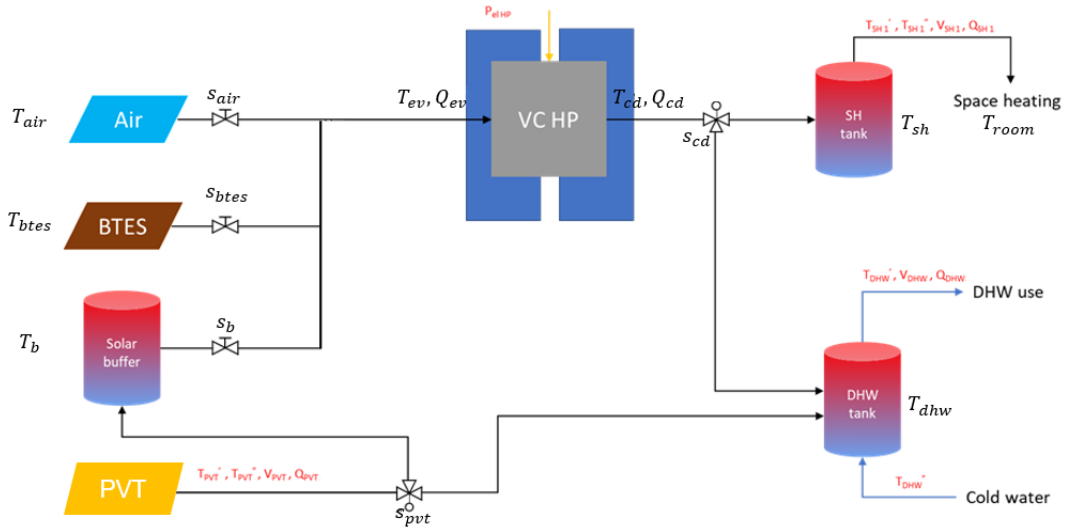


*Figure 3 Schematic overview of the vapour compression heat pump with three different sources (air, BTES and solar tank) in combination with PVT collectors, space heating and domestic hot water tank*

The parameters of the main system components in Figure 3 are given in Table 1. These parameters have been extracted from the actual components installed in the energy system and are used in the optimization problem described next.

*Table 1. System parameters*

| Component | Parameter | Real-life operation |
|---|---|---|
| **Vapour compression heat pump** | Max. thermal output | 15.5 kW |
| **Solar buffer** | Volume | 396 l |
| **DHW tank** | Volume layer 1 (bottom)<br>Volume layer 2 (top) | 41.7 l<br>207.5 l |
| **SH tank** | Volume | 396 l |
| **BTES field (virtual)** | Mass | 5211525 kg |
| **PVT collectors** | Surface | 8.6 $m^2$ |

The domestic hot water tank is considered to have two layers: bottom layer through which cold (tap) water enters the tank and the top layer through which hot water leaves the tank. The collectors always charge the bottom layer, while the heat pump charges the top layer.

The objective of the optimization is to optimize the operation of the heat pump for least energy consumption while ensuring the thermal comfort and DHW needs of the building occupants under the specified system constraints.

### 3.1 Optimisation problem

Before describing the optimization problem, all the variables, control inputs and system disturbances are introduced. The main optimization variables are defined in Table 2 and mainly represent the temperatures of the different system components.

*Table 2 Optimization variables*

| Variable | Definition |
|---|---|
| $T_{cd,out}$ | The output temperature from the heat pump condenser |
| $T_{cd,in}$ | The input temperature to the heat pump condenser |

| | |
|---|---|
| $T_{ev,out}$ | The output temperature from the heat pump evaporator |
| $T_{ev,in}$ | The input temperature to the heat pump evaporator |
| $T_{pvt,out}$ | Output temperature of the PVT collectors |
| $T_{pvt,in}$ | Input temperature to the PVT collectors |
| $T_b$ | Temperature of the water in the solar buffer |
| $T_{btes}$ | Temperature of the virtual BTES tank (emulating a BTES field) |
| $T_{sh}$ | Temperature of the space heating tank |
| $T_{dhw,1}$ | The temperature of the bottom layer in the hot water tank |
| $T_{dhw,2}$ | The temperature of the top layer in the hot water tank |

The main control variables are defined in Table 3. These represent the variables for controlling the operational temperature setpoint of the heat pump condenser output and the binary variables for controlling the valves that are responsible for the different heat pump and PVT connections.

*Table 3 Optimization control variables*

| Variable | Definition |
|---|---|
| $z_{ev,air}$ | Binary control that selects air as evaporator source |
| $z_{ev,btes}$ | Binary control that selects BTES as evaporator source |
| $z_{ev,solar}$ | Binary control that selects solar buffer as evaporator source |
| $z_{cd}$ | Binary control that selects what the HP charges (0-SH, 1-DHW tank) |
| $z_{pvt}$ | Binary control that selects what the PVT charges (0-Solar buffer, 1-DHW tank) |
| $T_{cd,oper}$ | The temperature set-point in the output of the condenser |

The system disturbances (or external inputs) are defined in Table 4. They represent the four main system disturbances that need to be forecasted: the domestic hot water and space heating demand, the outdoor temperature and the global solar irradiance.

*Table 4 Disturbances/external inputs to the optimization problem*

| Variable | Definition |
|---|---|
| $Q_{dhw}$ | Domestic hot water demand |
| $Q_{sh}$ | Space heating demand |
| $T_{\infty}$ | Outdoor temperature |
| $I_g$ | Global solar irradiance |

Using these definitions, the optimization problem with objective of minimizing the electricity consumption of the heat pump ( Eq. 1), to achieve energy savings subject to different system constraints (Eq. 2 to Eq. 8), by using the thermal flexibility of the space heating and hot water tanks to store heat is defined.

$$minimize \sum_{k=1}^{N+1} \dot{m}_{cd}\, c_{p,cd} \left(T_{cd,out,k} - T_{cd,in,k}\right) - \dot{Q}_{ev,emp} \left(T_{cd,out,k}, T_{ev,in,k}, z_{ev,k}\right) \quad \text{Eq. 1}$$

$$subject\ to\ F\left(\dot{\boldsymbol{T}}_k, \boldsymbol{T}_k, T_{cd,oper,k}, \boldsymbol{z}_k, Q_{dhw,k}, Q_{sh,k}, T_{\infty,k}, I_{g,k}\right) = 0, for\ k = 1, \dots N, \quad \text{Eq. 2}$$

$$z_{ev,k}, k \in \{0,1\} \times \{0,1\} \times \{0,1\}, for\ k = 1, \dots, N, \quad \text{Eq. 3}$$

$$z_{cd,k}, k \in \{0,1\} \times \{0,1\}, for\ k = 1, \dots, N, \quad \text{Eq. 4}$$

$$z_{pvt}, k \in \{0,1\}, for\ k = 1, \dots, N, \quad \text{Eq. 5}$$

$$z_{ev,btes,k} + z_{ev,solar,k} + z_{ev,air,k} = 1\ for\ k = 1, \dots, N, \quad \text{Eq. 6}$$

$$\boldsymbol{T}_{min} \leq \boldsymbol{T}_k \leq \boldsymbol{T}_{max}\ for\ k = 1, \dots, N, \quad \text{Eq. 7}$$

$$T_{cd,oper,min} \leq T_{cd,oper,k} \leq T_{cd,oper,max}\ for\ k = 1, \dots, N. \quad \text{Eq. 8}$$

where:

- $\dot{m}_{cd}$ and $c_{p,cd}$: mass flow rate and specific heat capacity of water in the condenser circuit.
- The electrical power of the heat pump is assumed to be equal to the difference between the power provided by the condenser and the power in the evaporator (neglecting any heat losses, with the heat pump tests confirming that this is a valid assumption).
    - The thermal power on the evaporator side $\dot{Q}_{ev,emp}(\cdot)$ is given by an equation-fit correlation that has been produced after processing the heat pump measurements. This correlation includes parameters that are different and depend on whether the evaporator source is water ( Eq. 9) or air ( Eq. 10).

$$\dot{Q}_{ev,emp,w} = a_0 + a_1 T_{ev,in} + a_2 T_{cd,out} \quad \text{Eq. 9}$$

$$\dot{Q}_{ev,emp,a} = b_0 + b_1 T_{ev,in} + b_2 T_{cd,out} \quad \text{Eq. 10}$$

    - The thermal power in the condenser has a straightforward equation ( Eq. 11), and based on the heat pump characterisation process, an equation-fit model has been developed for both water ( Eq. 12) and air source operation ( Eq. 13).

$$\dot{Q}_{cd} = \dot{m}_{cd}\, c_{p,cd} \left(T_{cd,out} - T_{cd,in}\right) \quad \text{Eq. 11}$$

$$\dot{Q}_{cd,emp,w} = c_0 + c_1 T_{ev,in} + c_2 T_{cd,out} \quad \text{Eq. 12}$$

$$\dot{Q}_{cd,emp,a} = d_0 + d_1 T_{ev,in} + d_2 T_{cd,out} \quad \text{Eq. 13}$$

Table 5 provides the values of the different parameters used to describe the thermal power of the evaporator and condenser. These values have been determined by experimentation in the laboratory.

*Table 5 Parameters describing the power in the evaporator and condenser sides of the heat pump.*

| Parameter | Water-source | Parameter | Air-source |
|---|---|---|---|
| $a_0$ | 9.921482107694256E+00 | $b_0$ | 9.14582553491968E+00 |
| $a_1$ | 2.537262914174811E-01 | $b_1$ | 2.4858957958198985E-01 |
| $a_2$ | -4.463182115681360 6E-02 | $b_2$ | -5.860872076898898E-02 |

| | | | |
|---|---|---|---|
| $c_0$ | 9.21291870167665E+00 | $d_0$ | 9.613824026447336E+00 |
| $c_1$ | 2.61772791010E-01 | $d_1$ | 2.5629891562259144E-01 |
| $c_2$ | 3.2727904136326834E-02 | $d_2$ | 1.300806756199765E-02 |

- $\boldsymbol{T}$ is the vector of all temperature variables, i.e. [$T_{cd,out}$, $T_{cd,in}$, $T_{ev,out}$, $T_{ev,in}$, $T_{pvt,out}$, $T_{pvt,in}$, $T_b$, $T_{sh}$, $T_{dhw,1}$, $T_{dhw,2}$]
- $\boldsymbol{z}_{ev} = [z_{ev,btes}, z_{ev,solar}, z_{ev,air}]^\top$ is the vector of binary variables that determine the power in the evaporator.
- $\boldsymbol{z}_{cd} = [z_{cd}, z_{cd,oper}]^\top$ is the vector of binary variables that determine the power in the condenser.
- $\boldsymbol{z} = [\, z_{ev,btes}, z_{ev,solar}, z_{ev,air}\,, z_{cd}, z_{pvt}]^{\,T}$ is the vector of all binary variables.
- Eq. 2 i.e., F(·) = 0, describes the dynamics of the system. Details on the system dynamics are provided in [42].
- $N$ is the number of control timesteps or the optimization horizon
- Eq. 3 to Eq. 6 ensure that the binary control variables take the permitted values.
- Eq. 7 imposes upper and lower bounds on the temperature states.
- Eq. 8 imposes bounds on the main control variable.

It is worth mentioning that the optimization problem described above is a mixed-integer non-linear programming problem, which can be difficult to solve. This becomes an issue especially when used in real-time control during field tests with priority to ensure the thermal comfort of the building's occupants; if the optimization problem does not reach a solution at a given control interval, no control signals will be issued and this could lead to occupant discomfort. Thus, a pure non-linear approximation of the problem was derived. In this approximation, the integer constraints on the decision variables were relaxed i.e. instead of a decision variable that selects a specific source for the evaporator during the whole control interval, the optimization allows to select as source a mixture of the various sources available during a control interval. In terms of power supplied by each source, this is addressed by further splitting the control interval according to the proportion required by each source, and the source switching is done accordingly. This formulation gives a purely non-linear model where the accuracies of each of the system models is not compromised.

### 3.2 Control setup/strategy

The optimization problem described in the previous section is solved using model predictive control (MPC) [12], which solves an optimization problem by computing optimal control signals at each control interval while ensuring that a set of input and state constraints are satisfied and minimizing a specific objective. The algorithm uses the receding horizon control approach with control signals computed at every control interval and the optimization horizon shifted forward at each control step. Feedback into the system through state estimation allows to correct any deviations of the prediction from reality by updating the initial conditions of the system with measurements or estimates of the system parameters. Figure 4 shows a schematic overview of the MPC process.

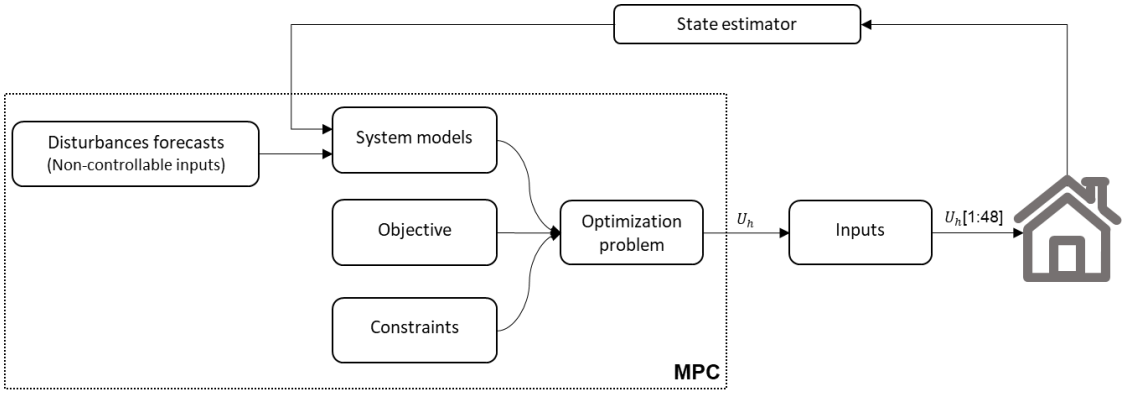


*Figure 4 Schematic overview of MPC*

A data-driven forecaster was developed to forecast the space heating demand. The forecaster relied on historical measurements of the space heating demand, and historical and forecast information of the outdoor temperature as input features as shown in Table 6. During the real-life operation, the forecaster was retrained once every day (in the morning) using historical data from the last 60 days. New predictions were made every hour.

*Table 6. Input features of space heating forecaster (D+X = current timestep + X days)*

| **Feature name** | **D+1** | **D-1** | **D-2** | **D-7** |
|---|---|---|---|---|
| Forecasted outdoor temperature [°C] | X | X | X | X |
| Measured SH demand [W] | - | X | X | X |
| Hour of the day | X | - | - | - |

A fixed residential DHW profile was used for the hot water consumption. Thus, the hot water demand forecast was replaced by this profile. The solar irradiation forecast was obtained from the commercial forecasting service of Rebase energy [43] and the outdoor temperature forecast from the Norwegian Meteorological Institute [44].

The MPC controller generates optimal energy profiles for charging the space heating and the DHW tanks for the next 24 hours with a control interval of 30 minutes. These profiles indicate the optimal energy that should be taken from the BTES, air or solar tank to charge the space heating ($\tilde{Q}_{sh}$) and hot water ($\tilde{Q}_{dhw}$) tanks, to meet the building demand. A profile on the optimal energy from the PVT to charge either the solar tank or the hot water tank is also generated. These profiles are then sent to the cloud controller, which in turn sends the optimal energy to the local BEMS controller in real-time at each control timestep, $k$. The BEMS controller adjusts the temperature setpoints of the space heating and DHW tanks taking into account the temperature boundaries in

Table 7. The following rules are used for the DHW tank:

- If $\tilde{Q}_{dhw} > 0$, $T_{set}$ is set to 51 °C until the accumulated heat, $Q$, charged into DHW tank reaches $\tilde{Q}_{dhw}$
- If $\tilde{Q}_{dhw} = 0$, $T_{set}$ is set to 46 °C, which ensures that an adequate amount of heat is always present in the tank to supply the hot water needs of the building.

*Table 7. Buffer temperature boundaries*

| Component | Temperature boundaries |
|---|---|
| **Solar buffer** | Min: 0 °C, Max: 23 °C |
| **DHW tank** | Min: 10 °C, Max: 60 °C (bottom part of the tank)<br>Min: 46 °C, Max: 51 °C (top part of the tank) |
| **Space heating tank** | Min: 40 °C, Max: 52 °C |
| **BTES** | Min: 14 °C, Max: 21 °C |

Figure 5 provides an overview on how the control signals are deployed in the system. A similar set of rules is used for implementing control signals for the space heating tank.

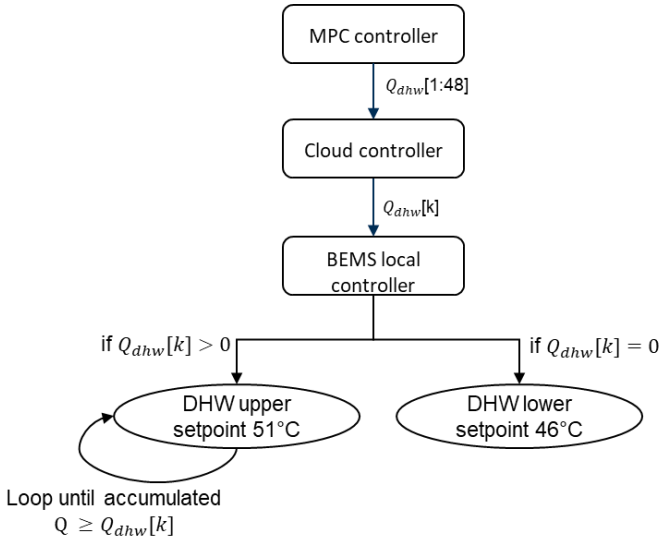


*Figure 5 Illustration of the deployment of the control signals issued by the MPC controller.*

## 4 Results

The pilot demonstration was carried out for a residential setup in Athens, Greece. An optimisation horizon of 24 hours was used with a control interval of 30 minutes. The field test with the BEMS control started at the beginning of winter 2022 with response tests and troubleshooting and became fully functional by the end of November 2022 running until the end of April 2023. The next sections discuss the results for the month of January (6/1/2023 – 31/1/2023) during the heating season, when the pilot was sorely controlled by the BEMS without any interruptions. Before the BEMS control went operational, the local control was occasionally handling the system operation serving as a benchmark to the BEMS control, to identify the energy savings potential.

### 4.1 Space heating and DHW forecasts

A comparison of the space heating measurement and forecast averaged per hour to obtain a representative day during January 2023 is shown in Figure 6. The space heating demand forecasts closely follows the actual space heating demand with a root mean square error (RMSE) of ≈1 kW throughout the month of January. The small deviations are due to the uncertainties in the user

behaviour, since the building is occupied by four people during the day. The peak of the demand in the morning (around 08:00 local time) is due to the sudden increase of the rooms' setpoint by 2 °C, requesting a significant amount of heat and for at least a 2-hour period.

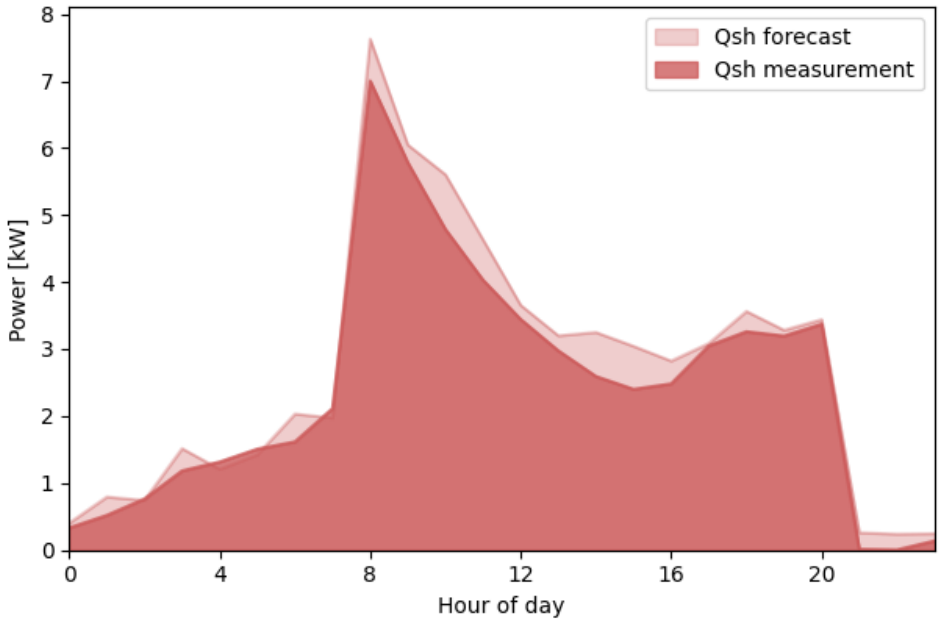


*Figure 6 Comparison of the daily average hourly space heating actual measurement and forecast for a representative day during the period 6/1/2023 – 31/1/2023*

Figure 7 shows a comparison of the profile used for the hot water demand and the actual measurements. The difference in these two profiles indicates the uncertainty in the inlet tap water temperature that slightly varies during the day and affects the provided heat demand profile. However, the RMSE is rather small and equal to ≈234 W. The tapping cycles closely follow the timing defined in the EN16147:2017, starting at around 07:00 in the morning and ending at almost 22:00 at night.

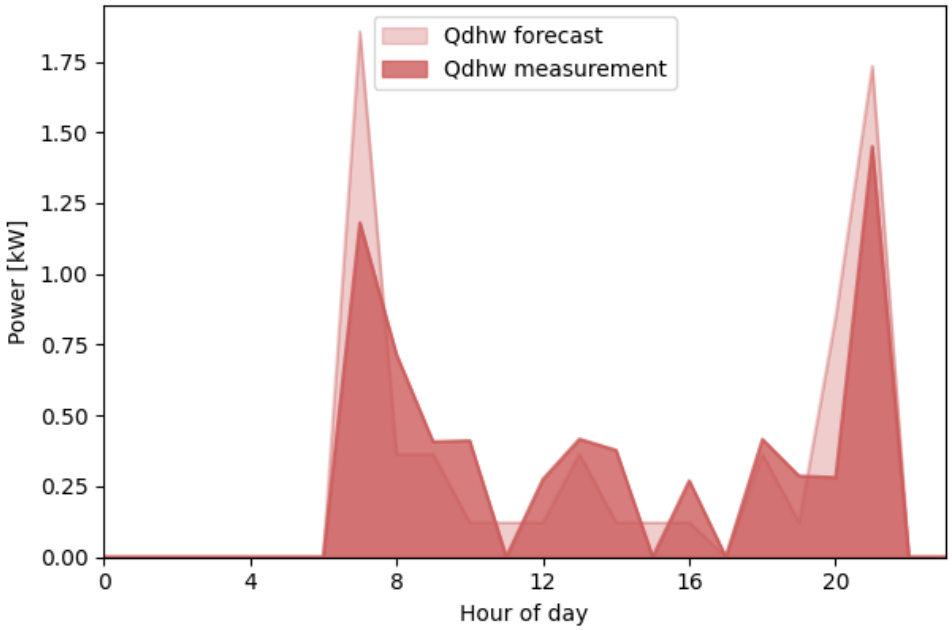


*Figure 7 Comparison of the daily average hourly hot water demand actual measurement and the profile for a representative day during the period 6/1/2023 – 31/1/2023.*

Overall, the daily cumulative energy demand from the forecast and real measurements for space heating and DHW are quite similar (forecasts vs. measurements: 64.04 vs. 57.82 kWh for space heating and 6.73 vs. 6.51 kWh for DHW), revealing the reliability of the two forecasters, which is a critical aspect in any MPC approach.

## 4.2 Optimization results

In this section the optimization results are discussed by looking at the daily average for the whole test period in January and a specific day (9/1/2023) that has similar weather conditions to those of a test day with the local control, which serves as a benchmark to identify the benefits introduced by the optimized control.

### 4.2.1 Heat sources of the heat pump

The first part of the optimization results discusses how the different heat sources of the heat pump are selected by the controller. The relative time spent by the heat pump with the different sources (air, BTES or solar buffer) to provide heat for space heating are shown in Figure 8 (monthly average) and Figure 9 (specific day 9/1/2023). Similar plots for the domestic hot water are shown in Figure 10 and Figure 11. The heat pump operates for charging the DHW tank (the top layer) only a few times in a day as shown in Figure 11, due to the relatively low demand and the low tank volume. However, since this occurs at different periods of each day, the average shown in Figure 10 is obtained.

As shown on the plots, most of the heat for space heating and hot water provision is supplied by the heat pump with the BTES as its main source of heat. During the days with sunshine, the solar buffer is charged by the PVT collectors at a temperature higher than that of the BTES (typically after 11:00 in the morning), causing the controller to select the solar buffer as the heat source to the heat pump even in the evening hours (e.g. at 21:00-22:00). Air as a heat source to the heat pump is never used due to the low outdoor air temperatures in winter, with the use of the virtual BTES favoured due to its constant temperature of 18 °C (air source would be favoured if ambient temperature would have been about 7-8 K higher than the BTES temperature).

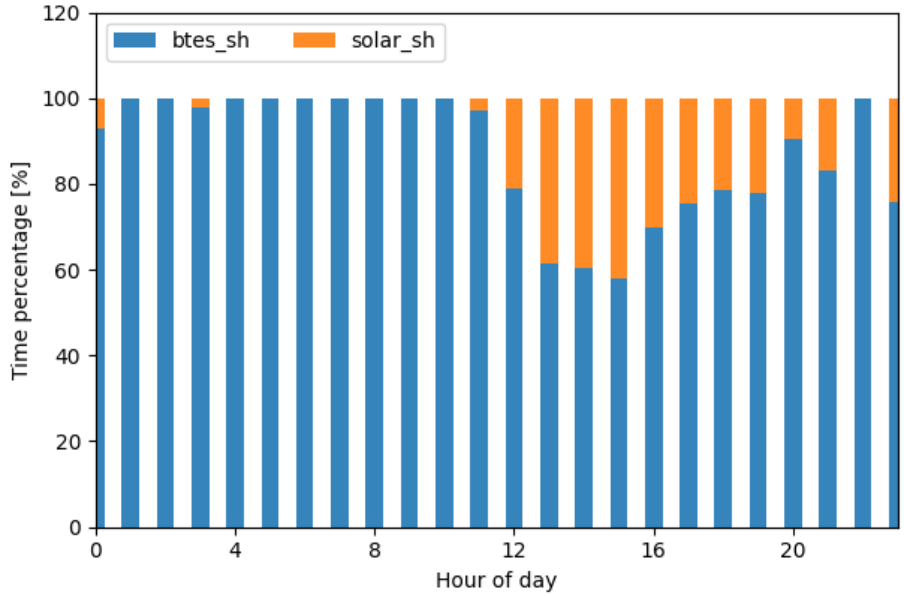


*Figure 8 Daily average relative time of sources used by the heat pump for space heating– 6/1/2023 – 31/1/2023*

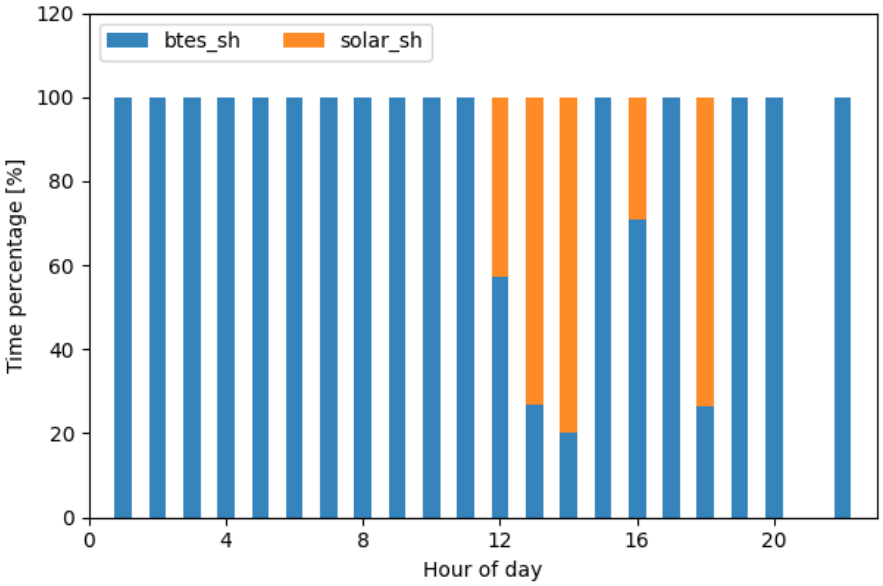


*Figure 9 Relative time spent by the heat pump with the different sources for space heating on a specific test day – 9/1/2023*

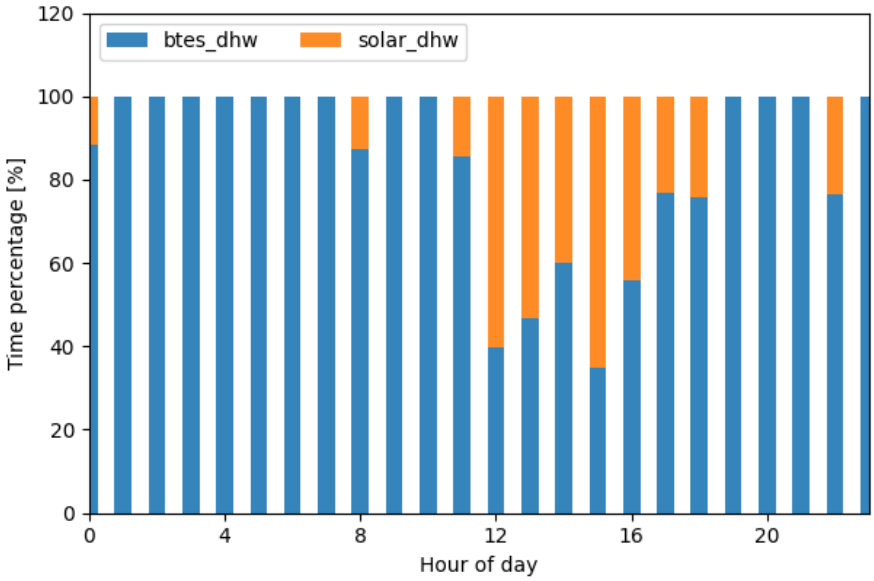


*Figure 10 Daily average relative time of sources used by the heat pump for hot water provision – 6/1/2023 – 31/1/2023*

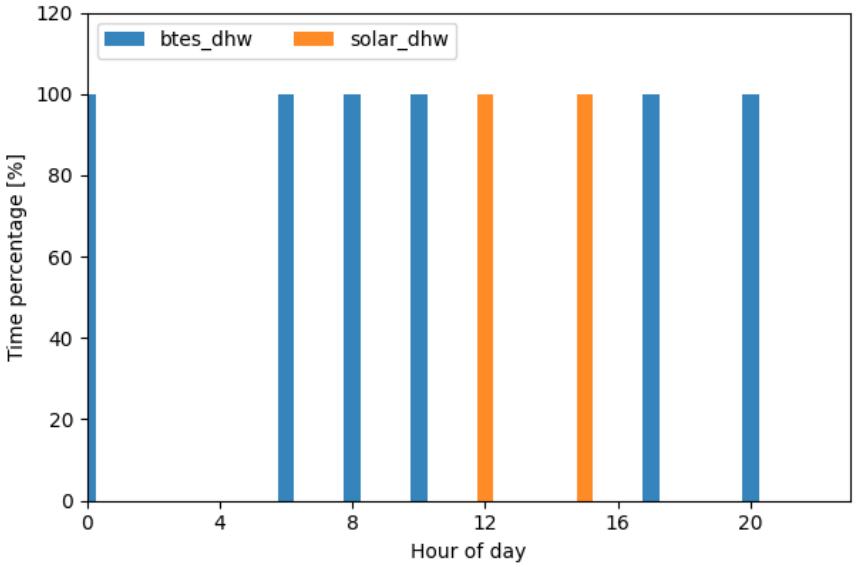


*Figure 11 Relative time spent by the heat pump with the different sources for hot water provision on a specific test day – 9/1/2023*

Regarding the interactions between the PVT collectors with the solar buffer and the DHW tank, the collectors directly charge the DHW tank for very limited periods during the day (this occurred only once in January at early afternoon). This is because the solar fluid temperature of the collectors is not high enough to directly supply the DHW tank due to the low ambient temperature that increases the heat losses of the collectors. The collectors were almost exclusively charging the solar buffer tank increasing its temperature, which was frequently discharged by the evaporator of the heat pump. It is worth mentioning that in the pilot demonstration, there was no neutral position setting for the valves. The solar pump of this circuit was actuated by an independent controller based on the temperature difference (inlet/outlet) of the collector field. When the solar pump was not running, the default position of the solar valve was set to direct the flow towards the solar buffer.

### 4.2.2 Tank temperatures

Figure 12 (daily average) and Figure 13 (specific day) show the evolution of the tank temperatures: space heating tank temperature ($T_{sh}$) and DHW tank temperatures ($T_{dhw1}$ for bottom of tank and $T_{dhw2}$ for top of tank), together with their minimum and maximum values. Both the space heating and hot water tanks are charged to high temperatures (45 °C and 49 °C respectively) in the morning due to the forecasted increase in the space heating and hot water demand as can be seen in Figure 6 and Figure 7. The space heating tank is operated at very stable temperatures and closer to its lower temperature setpoint for most of the day, which favours the heat pump COP. Thus, reducing the energy consumption and consequently the standing losses since this tank is installed outdoors. Similarly, the temperature of the top layer of the DHW tank fluctuates around 45-46 °C for most parts of the day, which is the minimum temperature for keeping the tap outlet temperature in the proximity of 45 °C, which is the targeted value. However, in the morning, the DHW tank temperature falls below the minimum setpoint because the tank was not charged enough (49°C for the daily average and 47 °C on a specific day) to meet the peak hot water demand in the morning, when there are frequent tapping cycles (4 in total starting from 07:15 and ending at 08:45). The thermal power discharged during each cycle is around 10 kW, causing a sudden drop to the tank temperature. This triggers the heat pump operation, but its starting sequence requires about 2 minutes (e.g. to allow the complete change of the valves' direction), which is enough for the temperature to drop below the minimum value. The bottom layer of the DHW tank remains inactive during this period because it is not charged by the collectors during that day and any variation of its temperature is caused by the water mixing within the tank during the tapping cycles.

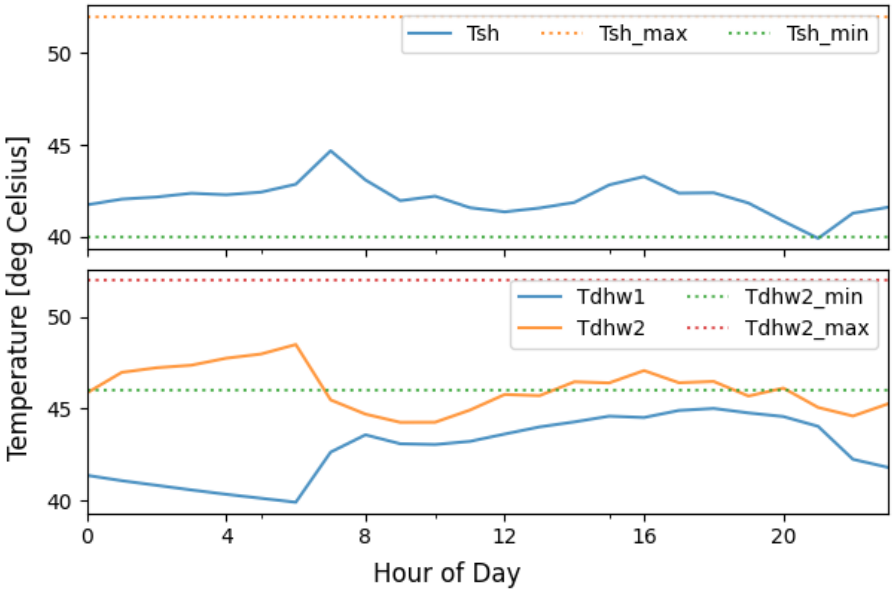


*Figure 12 Daily average tank temperatures – 6/1/2023 – 31/1/2023*

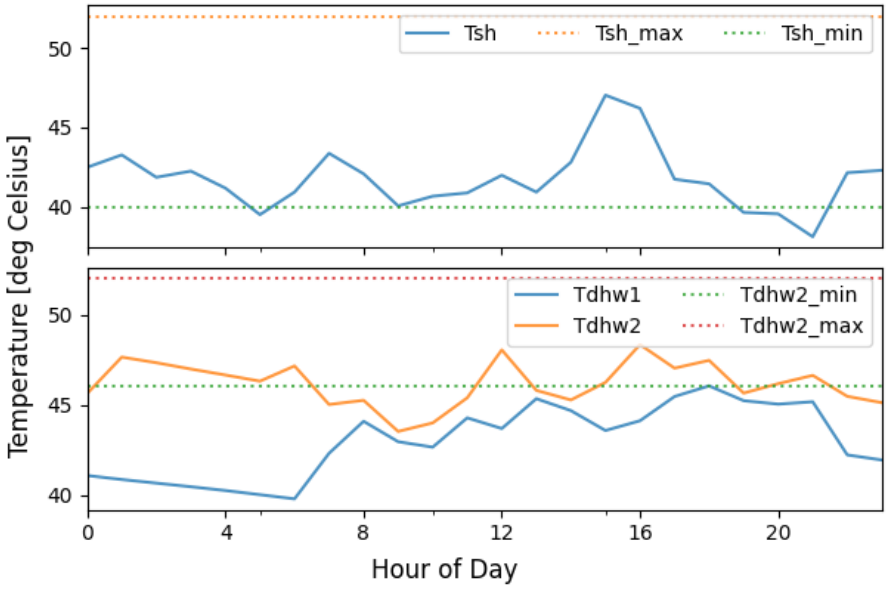


*Figure 13 Tank temperatures on a specific test day - 9/1/2023*

### 4.2.3 Performance and energy flows

Table 8 summarises the results over the period 6/1/2023 – 31/1/2023, by giving the main heat and electricity flows in the system. A significant amount of the building heat demand is served by the heat pump, since only a very small share of DHW demand is covered directly by the PVT collectors, as previously explained. Moreover, the available heat from the solar buffer represents a small share of around 18% of the total heat source to the heat pump (around 40 kWh per day). In case the system layout did not consider the use of a (virtual) BTES field, this share would have increased, favouring the use of this source instead of air for a longer duration. This would also favour the collector efficiency, which would operate at an even lower temperature with less heat losses. In terms of electricity flows, the PVT electricity generation is much less compared to the heat pump electricity consumption due to winter conditions (the collectors produce around 4 kWh in a typical summer day). Since the optimization objective is geared towards minimizing electricity consumption of the heat pump and

not self-consumption of the local electricity generation, a detailed discussion of this result is out of the scope of this work.

*Table 8 Summary of results over the period 6/1/2023 – 31/1/2023*

| | **Heat load for SH and DHW [kWh]** | **Total heat of HP [kWh]** | **HP total electricity consumption [kWh]** | **Heat PVT to solar buffer [kWh]** | **Heat PVT to DHW tank [kWh]** | **Electricity PVT [kWh]** |
|---|---|---|---|---|---|---|
| **Daily average** | 64.31 | 64.95 | 25.13 | 7.24 | 0.04 | 1.88 |
| **6/1/2023 – 31/1/2023** | 1672.07 | 1688.76 | 653.34 | 188.19 | 1.07 | 48.79 |

The heat production of the heat pump for charging the two tanks is higher than the actual load due to heat losses. These become significant in winter since many parts of the installation are outdoors (space heating tank, fan coils pump, piping and 3-way valves) and have been estimated to about 4% from the whole piping circuit and 1% from the tank. The electricity consumption of the heat pump includes all stand-by (≈130 W) and auxiliary (≈110 W) power consumption. During operation, these values are much lower than the compressor power (which is ≈4-4.5 kW) and are usually neglected. However, here the calculated heat pump performance includes all power consumptions of the heat pump.

Figure 14 (daily average) and Figure 15 (specific day) indicate the main heat flows of the system. $Q_{cd\_sh}$ and $Q_{cd\_dhw}$ represent the heat provided by the heat pump to the space heating and the DHW tanks respectively (values given in kWh). Peak heat production by the heat pump condenser occurs in the morning to meet the peak heating load. As mentioned earlier, most of the heat production by the PVT collectors charges the solar buffer ($Q_{pvt\_solar\_buffer}$ ) with a very limited amount directly charging the DHW tank ($Q_{pvt\_dhw}$).

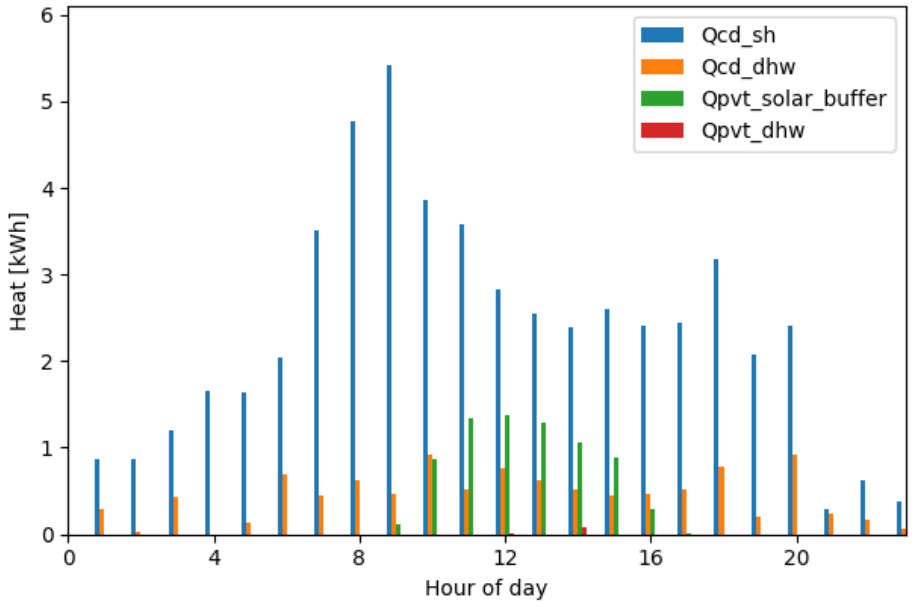


*Figure 14 Daily average system heat flows: heat produced by the heat pump for space heating ($Q_{cd\_sh}$) and domestic hot water supply ($Q_{cd\_dhw}$), heat produced by the PVT collectors for charging the DHW tank ($Q_{pvt\_dhw}$) and the solar buffer ($Q_{pvt\_solar\_buffer}$) – 6/1/2023 – 31/1/2023.*

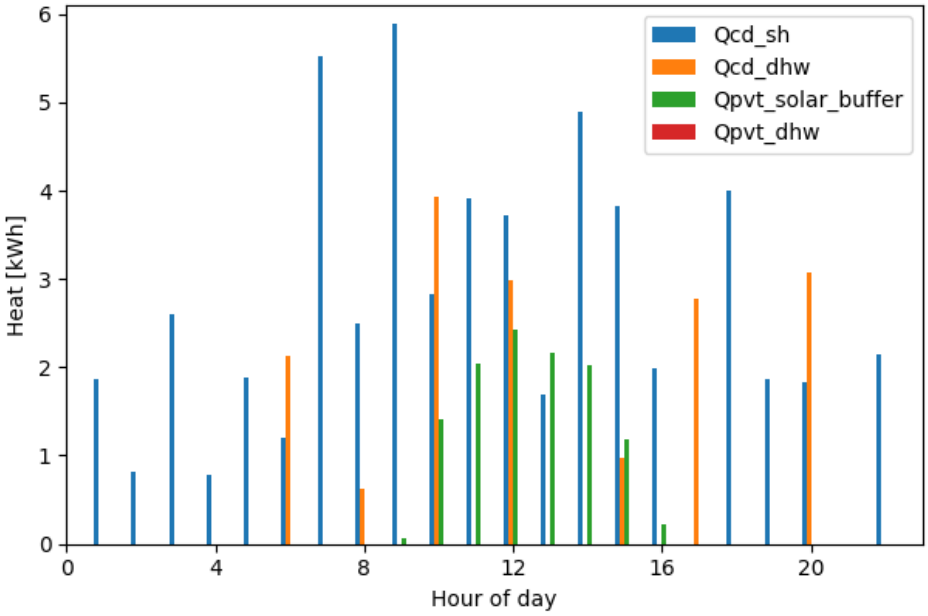


*Figure 15 System heat flows: heat produced by the heat pump for space heating ($Q_{cd\_sh}$) and domestic hot water supply ($Q_{cd\_dhw}$), heat produced by the PVT collectors for charging the DHW tank ($Q_{pvt\_dhw}$) and the solar buffer ($Q_{pvt\_solar\_buffer}$) - specific test day 9/1/2023.*

The COP of the heat pump varies throughout the day during its operation as shown in Figure 16 and Figure 17 when the heat pump is serving the space heating and DHW tanks respectively. The COP is always greater 2 in both modes of operation averaging to 3.37 for space heating operation and 3.58 for the DHW operation throughout the January test period. With most of the solar heat used for charging the solar buffer, this leads to an increase in the heat pump COP when the solar buffer is the heat source because the temperature of the water from the solar buffer is higher than the BTES field temperature. However, this happens a few times per day, with the performance enhancement being small. This improvement is observed around the noon hours, when the COP for space heating approaches or even exceeds values of 3.5. Finally, a very low COP is observed especially very early in the morning because the heat pump operates for very few minutes, with the start/stop sequence contributing to the auxiliary consumption and the heating up of the heat exchangers.

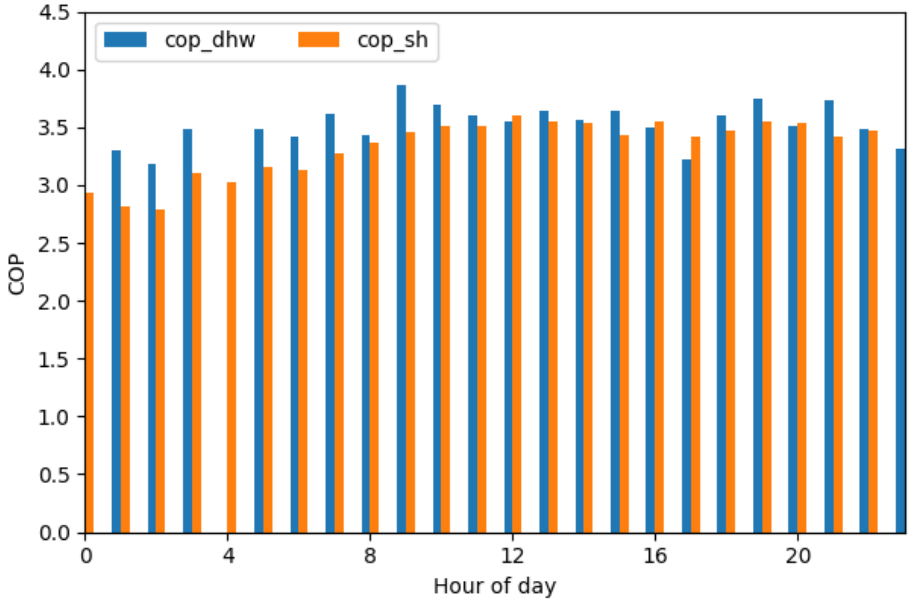


*Figure 16 Average heat pump COP for space heating and hot water – 6/1/2023 – 31/1/2023*

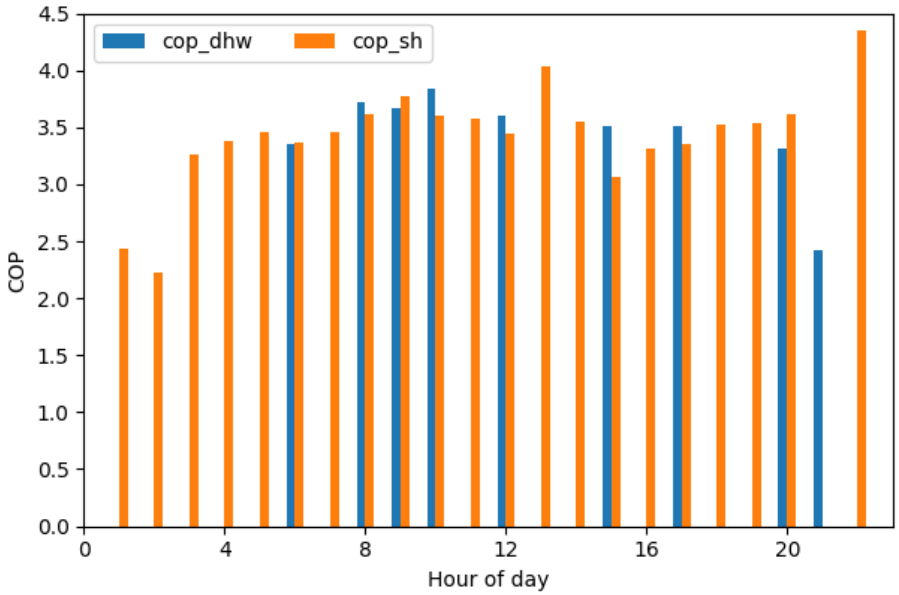


*Figure 17 Heat pump COP for space heating and hot water provision – specific test day 9/1/2023*

### 4.2.4 Comparison of BEMS with local control over a one-day operation period

Table 9 compares the operation of the BEMS and the local control (business-as-usual mode of operation) of the system, using the daily values from the system operation on two days (4/1/2023 for local control and 9/1/2023 for the BEMS control) with similar weather conditions. Even though both days have a similar average outdoor temperature and total solar radiation (on all collectors with a surface of 8.6 $m^2$), there is a 3.55 kWh difference in the heat demand (≈5%). This could be caused by the higher solar radiation during the day that the BEMS control was active and the user behaviour. Despite the DHW heat demand on the day with BEMS control being slightly higher, overall the heat pump electricity consumption is reduced with the BEMS control by 7%. Notice that with the BEMS control, the heat pump operates at a slightly higher COP for both space heating and DHW, because it is able to charge the tanks at smaller steps while also keeping the tanks at lower average temperatures (closer to their lower bounds). It should be stressed that a similar trend is observed during all other days regarding the COP and electricity consumption for space heating.

*Table 9 Comparison of BEMS with local control*

| Daily values | Local control – 04/01/2023 | BEMS control – 09/01/2023 |
|---|---|---|
| Average outdoor temperature [°C] | 8.73 | 8.63 |
| Solar radiation [kWh] | 41.55 | 42.20 |
| PVT heat total [kWh] | 12.12 | 11.40 |
| PVT heat to DHW [kWh] | 0.00 | 0.00 |
| PVT electricity [kWh) | 2.45 | 2.52 |
| DHW heat demand [kWh] | 6.51 | 6.73 |
| Building heating demand [kWh] | 69.81 | 66.26 |
| HP electricity consumption [kWh] | 28.76 | 27.00 |
| COP for DHW [-] | 3.16 | 3.39 |
| COP for SH [-] | 3.35 | 3.37 |
| COP total [-] | 3.25 | 3.38 |

### 4.2.5 Comparison of BEMS with local control over the whole winter period

The field tests were conducted over the whole winter period of 2022-2023, developing correlations that provide the daily electricity consumption of the heat pump for space heating ($P_{HP\ heat}$) as a function of the daily ambient temperature (independent variable with the highest effect on this consumption). Different correlations were developed for local and BEMS control, given by (Eq. 14) and (Eq. 15) respectively (fitting accuracy with $R^2$ of around 75%).

$$P_{HP,heat-LOCAL} = 4.31840721E+01 - 2.80338668E+00\ T_{amb} + 3.44482156E-02\ T_{amb}^2$$

*Eq. 14*

$$P_{HP,heat-BEMS} = 3.48982505E+01 - 1.82584030E+00\ T_{amb} + 1.13760238E-02\ T_{amb}^2$$

*Eq. 15*

Where $T_{amb}$ is the average daily ambient temperature (in °C) and the electricity consumption is given in kWh/day.

Using these two correlations and the measured data collected during the entire testing period (November 2022 to mid of April 2023), the results are given in Figure 18 i.e. heat pump electricity consumption for space heating as a function of the daily ambient temperature. It should be highlighted that the available data include temperatures from around 5 °C up to almost 18 °C.

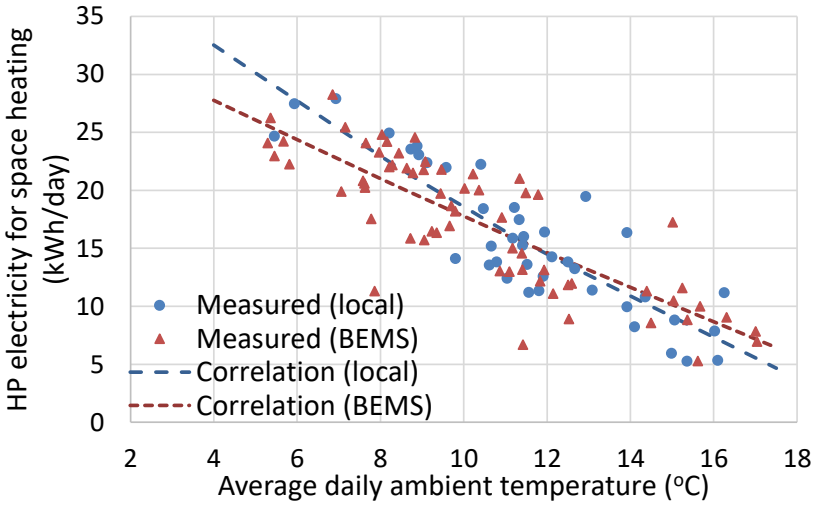


*Figure 18 Measured and correlated daily electricity consumption of the heat pump for space heating for the two control modes*

Most of the days are characterised by daily ambient temperatures in the range of 8-12 °C with few days below 6 °C. Based on Figure 18, it becomes clear that the BEMS reduces the electricity consumption of the heat pump compared to the local control especially during the colder days, when the building load is high and the negative effect of frequent start/stop occasions becomes negligible. The opposite is observed during warmer winter days, when the heat pump operates few times per day. In this case, it is preferrable to fully charge the space heating tank instead of forcing the charging process to follow the minimum allowed tank setpoint.

## 5 Conclusions and lessons learned

This paper has discussed the use of MPC in a real-life operational control of a multi-source heat pump to leverage flexibility from heat pump heat sources, space heating and domestic hot water tanks for energy savings. The MPC controller relies on forecasts of the weather, space heating and hot water demand, together with the system constraints to make optimal decisions on how much heat to take

from each of the input sources (air, BTES or solar buffer), which tank (space heating or hot water) to serve and which tank (solar buffer or domestic hot water tank) to direct the output of the PVT collectors to. This emphasizes the importance of accurate forecasts as they have a direct impact on the quality of the controller output/decisions. For the field test during almost one winter month (January 2023), the developed space heating demand data-driven forecaster achieved a RMSE of around 1 kW. A fixed hot water demand profile was used in the field tests. However, a RMSE of 234 W was observed between the actual and the expected measurements. These show that there is always some inherent uncertainty around user-behaviour and weather forecast, which cannot be completely solved even by imposing a fixed pattern on the users. Therefore, it would be interesting to explore different ways on how to model and incorporate this uncertainty in the forecaster itself or when solving the optimisation problem.

Results from the field test have demonstrated the potential and added value of MPC via a building energy management system. The BEMS control led to a ≈7% reduction in the heat pump electricity consumption compared to the business-as-usual control (with similar number of heat pump start/stop cycles). The main challenge of MPC experienced in this project is the significant amount of effort required to develop sufficiently accurate white-box models of the different system components. This reduces the replicability of the algorithm in buildings without the exact same system components. A future step would be to move towards physics-informed data-driven system modelling, adapting and using the standard/simplified physical equations as a starting point for machine learning techniques together with data from system operation for learning the system dynamics. This would significantly reduce the resources required for system modelling without compromising the model accuracy after the training period is finalised.

The field test also showed the importance of a fallback controller when there was a communication failure or other issues that led to control signals not being issued or sent. Without a fallback controller, the end-users would potentially experience some discomfort, which affects their willingness to accept smart control in their buildings.

These outcomes from the field test serve as proof of the potential of MPC via BEMS in buildings with real user behaviour, paving the way for further developments and improvements. The focus has been on energy savings without considering self-consumption of the local generation or cost of buying/injecting power to the grid. Thus, an immediate future step would be to consider multi-objective optimisation combining energy savings and self-consumption of the local generation taking also into account the cost of injecting/drawing power to/from the grid.

## Acknowledgements

This work has been performed in the context of the RES4BUILD project (Renewables for clean energy buildings in a future power system) – Horizon 2020 program, Grant Agreement no. 814865.

## References

[1] International Energy Agency, “Renewables 2022 Analysis and forecast to 2027,” 2023. Accessed: Feb. 07, 2023. [Online]. Available: https://iea.blob.core.windows.net/assets/ada7af90-e280-46c4-a577-df2e4fb44254/Renewables2022.pdf

[2] European Commission, “REPowerEU: A plan to rapidly reduce dependence on Russian fossil fuels and fast forward the green transition,” 2022. https://ec.europa.eu/commission/presscorner/detail/en/IP_22_3131 (accessed Feb. 07, 2023).

[3] D. O. Cabral, “Photovoltaic-Thermal Solar Collectors – A Rising Solar Technology for an Urban Sustainable Development,” in *Urban Transition - Perspectives on Urban Systems and Environments [Working Title]*, IntechOpen, 2022. doi: 10.5772/intechopen.104543.

[4] A. S. Gaur, D. Z. Fitiwi, and J. Curtis, “Heat pumps and our low-carbon future: A comprehensive review,” *Energy Res Soc Sci*, vol. 71, p. 101764, Jan. 2021, doi: 10.1016/j.erss.2020.101764.

[5] S. K. Pathak, P. O. Sharma, V. Goel, S. Bhattacharyya, H. Ş. Aybar, and J. P. Meyer, “A detailed review on the performance of photovoltaic/thermal system using various cooling methods,” *Sustainable Energy Technologies and Assessments*, vol. 51, p. 101844, Jun. 2022, doi: 10.1016/j.seta.2021.101844.

[6] P. A. Fokaides and A. M. Papadopoulos, “Cost-optimal insulation thickness in dry and mesothermal climates: Existing models and their improvement,” *Energy Build*, vol. 68, no. PARTA, pp. 203–212, Jan. 2014, doi: 10.1016/J.ENBUILD.2013.09.006.

[7] T. E. Seghier, Y. W. Lim, M. F. Harun, M. H. Ahmad, A. A. Samah, and H. A. Majid, “BIM-based retrofit method (RBIM) for building envelope thermal performance optimization,” *Energy Build*, vol. 256, p. 111693, Feb. 2022, doi: 10.1016/J.ENBUILD.2021.111693.

[8] T. Cholewa *et al.*, “On the forecast control of heating system as an easily applicable measure to increase energy efficiency in existing buildings: Long term field evaluation,” *Energy Build*, vol. 292, p. 113174, Aug. 2023, doi: 10.1016/J.ENBUILD.2023.113174.

[9] H. Thieblemont, F. Haghighat, R. Ooka, and A. Moreau, “Predictive control strategies based on weather forecast in buildings with energy storage system: A review of the state-of-the art,” *Energy Build*, vol. 153, pp. 485–500, Oct. 2017, doi: 10.1016/J.ENBUILD.2017.08.010.

[10] F. Oldewurtel *et al.*, “Use of model predictive control and weather forecasts for energy efficient building climate control,” *Energy Build*, vol. 45, pp. 15–27, Feb. 2012, doi: 10.1016/J.ENBUILD.2011.09.022.

[11] B. Zhang, W. Hu, A. M. Y. M. Ghias, X. Xu, and Z. Chen, “Multi-agent deep reinforcement learning based distributed control architecture for interconnected multi-energy microgrid energy management and optimization,” *Energy Convers Manag*, vol. 277, p. 116647, 2023.

[12] J. Drgoňa *et al.*, “All you need to know about model predictive control for buildings,” *Annual Reviews in Control*, vol. 50. 2020. doi: 10.1016/j.arcontrol.2020.09.001.

[13] L. Kudela, M. Špiláček, and J. Pospíšil, “Multicomponent numerical model for heat pump control with low-temperature heat storage: A benchmark in the conditions of Central Europe,” *Journal of Building Engineering*, p. 105829, 2023.

[14] S. Noye, R. M. Martinez, L. Carnieletto, M. De Carli, and A. C. Aguirre, “A review of advanced ground source heat pump control: Artificial intelligence for autonomous and adaptive control,” *Renewable and Sustainable Energy Reviews*, vol. 153, p. 111685, 2022.

[15] J. Arroyo, C. Manna, F. Spiessens, and L. Helsen, “Reinforced model predictive control (RL-MPC) for building energy management,” *Appl Energy*, vol. 309, p. 118346, 2022.

[16] W. Wang, B. Hu, R. Z. Wang, M. Luo, G. Zhang, and B. Xiang, “Model predictive control for the performance improvement of air source heat pump heating system via variable water temperature difference,” *International Journal of Refrigeration*, vol. 138, pp. 169–179, 2022.

[17] B. S. Sadjjadi, J.-N. Gerdes, and A. Sauer, “Energy flexible heat pumps in industrial energy systems: A review,” *Energy Reports*, vol. 9, pp. 386–394, 2023.

[18] P. Hlanze, Z. Jiang, J. Cai, and B. Shen, “Model-based predictive control of multi-stage air-source heat pumps integrated with phase change material-embedded ceilings,” *Appl Energy*, vol. 336, p. 120796, 2023.

[19] W. Wang, B. Hu, R. Z. Wang, M. Luo, G. Zhang, and B. Xiang, “Model predictive control for the performance improvement of air source heat pump heating system via variable water temperature difference,” *International Journal of Refrigeration*, vol. 138, pp. 169–179, 2022.

[20] S. Rastegarpour, S. Gros, and L. Ferrarini, “MPC approaches for modulating air-to-water heat pumps in radiant-floor buildings,” *Control Eng Pract*, vol. 95, p. 104209, Feb. 2020, doi: 10.1016/J.CONENGPRAC.2019.104209.

[21] J. Salpakari and P. Lund, “Optimal and rule-based control strategies for energy flexibility in buildings with PV,” *Appl Energy*, vol. 161, pp. 425–436, Jan. 2016, doi: 10.1016/J.APENERGY.2015.10.036.

[22] Z. Lee, K. Gupta, K. J. Kircher, and K. M. Zhang, “Mixed-integer model predictive control of variable-speed heat pumps,” *Energy Build*, vol. 198, pp. 75–83, Sep. 2019, doi: 10.1016/J.ENBUILD.2019.05.060.
[23] S. Kuboth, F. Heberle, T. Weith, M. Welzl, A. König-Haagen, and D. Brüggemann, “Experimental short-term investigation of model predictive heat pump control in residential buildings,” *Energy Build*, vol. 204, p. 109444, Dec. 2019, doi: 10.1016/J.ENBUILD.2019.109444.
[24] R. M. Lazzarin, “Dual source heat pump systems: operation and performance,” *Energy Build*, vol. 52, pp. 77–85, 2012.
[25] R. Lazzarin and M. Noro, “Photovoltaic/Thermal (PV/T)/ground dual source heat pump: Optimum energy and economic sizing based on performance analysis,” *Energy Build*, vol. 211, p. 109800, 2020.
[26] Z. Han, L. Qu, X. Ma, X. Song, and C. Ma, “Simulation of a multi-source hybrid heat pump system with seasonal thermal storage in cold regions,” *Appl Therm Eng*, vol. 116, pp. 292–302, 2017.
[27] Y. Nam, R. Ooka, and Y. Shiba, “Development of dual-source hybrid heat pump system using groundwater and air,” *Energy Build*, vol. 42, no. 6, pp. 909–916, 2010.
[28] R. Lazzarin and M. Noro, “Lessons learned from long term monitoring of a multisource heat pump system,” *Energy Build*, vol. 174, pp. 335–346, 2018.
[29] H. Weeratunge, G. Narsilio, J. De Hoog, S. Dunstall, and S. Halgamuge, “Model predictive control for a solar assisted ground source heat pump system,” *Energy*, vol. 152, pp. 974–984, 2018.
[30] R. Roure, D. Chèze, and M. Vallée, “Model predictive control of sun-coupled innovative heat pumps: a comparison of economic and environmental optimizations,” *Open Research Europe*, vol. 3, no. 17, p. 17, 2023.
[31] “SunHorizon Project,” *https://sunhorizon-project.eu/*. https://www.horizon2020ideas.eu/ (accessed Jun. 16, 2023).
[32] F. Busato, R. Lazzarin, and M. Noro, “The Control of Renewable Energies to Improve the Performance of Multisource Heat Pump Systems: A Two-Case Study,” *Applied Sciences*, vol. 11, no. 14, p. 6653, 2021.
[33] S. Cesari *et al.*, “A heat pump-based multi-source renewable energy system for the building air conditioning: the IDEAS project experience,” *TECNICA ITALIANA*, vol. 65, no. 1, pp. 12–22, 2021.
[34] K. Kaygusuz and T. Ayhan, “Experimental and theoretical investigation of combined solar heat pump system for residential heating,” *Energy Convers Manag*, vol. 40, no. 13, pp. 1377–1396, 1999.
[35] “IDEAS Project.” https://www.horizon2020ideas.eu/ (accessed Jun. 16, 2023).
[36] “EXCESS Project,” *https://positive-energy-buildings.eu/*. www.res4build.eu (accessed Jun. 16, 2023).
[37] EXCESS Project, “Deliverable 3.4: EXCESS Model-Predictive Control Algorithms,” 2022.
[38] “RES4BUILD Project.” www.res4build.eu (accessed Jun. 16, 2023).
[39] M. Pilou, G. Kosmadakis, G. Meramveliotakis, and A. Krikas, “Renewable Energy Based Systems with Heat Pumps for Supplying Heating and Cooling in Residential Buildings,” in *in 34th International Conference on Efficiency, Cost, Optimization, Simulation and Environmental Impact of Energy Systems (ECOS 2021)*, Taormina, Italy, 2021. doi: 10.52202/062738-0114.
[40] G. Meramveliotakis, G. Kosmadakis, M. Pilou, and S. Karellas, “Testing a Flexible Configuration of a Solar-Assisted Heat Pump with PVT Collectors for Domestic Hot Water Production,” in *EuroSun 2022 - ISES IEA SHC Conf. Sol. Energy Build. Ind.* , Kassel, 2022.
[41] M. Pilou, G. Kosmadakis, G. Meramveliotakis, and A. Krikas, “Towards a 100% renewable energy share for heating and cooling in office buildings with solar and geothermal energy,” *Solar Energy Advances*, vol. 2, p. 100020, 2022, doi: 10.1016/j.seja.2022.100020.
[42] M. Pilou, G. Kosmadakis, and G. Meramveliotakis, “Modeling of an Integrated Renewable-Energy-Based System for Heating, Cooling, and Electricity for Buildings,” *Energies (Basel)*, vol. 16, no. 12, p. 4691, Jun. 2023, doi: 10.3390/en16124691.

[43] “Rebase energy.” https://www.rebase.energy/products/forecast (accessed Jun. 16, 2023).
[44] “Norwegian Meteorological Institute.” https://www.yr.no/en (accessed Jun. 16, 2023).